Organic Electronics 13 (2012) 697–704

Contents lists available at SciVerse ScienceDirect

Organic Electronics

journal homepage: www.elsevier.com/locate/orgel

Efficient inverted polymer solar cells incorporating doped organic electron transporting layer

Zai-Quan Xu [a], Jin-Peng Yang [a], Fu-Zhou Sun [a], Shuit-Tong Lee [b], Yan-Qing Li [a,*], Jian-Xin Tang [a,*]

[a] Jiangsu Key Laboratory for Carbon-Based Functional Materials & Devices, Institute of Functional Nano & Soft Materials (FUNSOM), Soochow University, Suzhou 215123, China

[b] Center of Super-Diamond and Advanced Films (COSDAF), Department of Physics and Materials Science, City University of Hong Kong, Hong Kong SAR, China

ARTICLE INFO

Article history:
Received 22 September 2011
Received in revised form 29 November 2011
Accepted 15 January 2012
Available online 31 January 2012

Keywords:
Polymer solar cell
Inverted structure
Organic electron transporting layer
n-Type doping

ABSTRACT

An efficient inverted polymer solar cell is enabled by incorporating an n-type doped wide-gap organic electron transporting layer (ETL) between the indium tin oxide cathode and the photoactive layer for electron extraction. The ETL is formed by a thermal-deposited cesium carbonate-doped 4,7-diphenyl-1,10-phenanthroline (Cs_2CO_3:BPhen) layer. The cell response parameters critically depended on the doping concentration and film thickness of the Cs_2CO_3:BPhen ETL. Inverted polymer solar cell with an optimized Cs_2CO_3:BPhen ETL exhibits a power conversion efficiency of 4.12% as compared to 1.34% for the device with a pristine BPhen ETL. The enhanced performance in the inverted device is associated with the favorable energy level alignment between Cs_2CO_3:BPhen and the electron-acceptor material, as well as increased conductivity in the doped organic ETL for electron extraction. The method reported here provides a facile approach to optimize the performance of inverted polymer solar cells in terms of easy control of film morphology, chemical composition, conductivity at low processing temperature, as well as compatibility with fabrication on flexible substrates.

1. Introduction

Polymer solar cells (PSCs) composed of a conjugated polymer:fullerene-derivative bulk heterojunction (BHJ) are becoming an alternative approach to truly clean and renewable energy sources, because of their attractive advantages such as solution-processable roll-to-roll fabrication, mechanical flexibility, and tenability of chemical properties [1–8]. Significant progress on the power conversion efficiency (PCE) in PSCs has been made in recent years via the incorporation of new materials [9–11], morphology control [12], interface engineering [8], and device fabrication processes [5]. For instance, a very encouraging device performance with the PCE of 8.13% has recently been reported by Solarmer [13]. However, further improvement in efficiency and stability of PSCs is still required for practical applications as a cost competitive and sustainable technology.

In general, the device performance of regular-structure PSCs, comprised of an BHJ active layer sandwiched between a transparent indium tin oxide (ITO) anode and a low-work-function metal cathode (e.g., Ca, Al) [1,3], degrades fast due to the acidic and hygroscopic nature of the hole collection layer of poly(3,4-ethylene dioxythiophene):(polystyrene sulfonic acid) (PEDOT:PSS) and the oxidation of the reactive metal cathode upon exposure to moisture and oxygen [1,14]. It had been demonstrated that the inverted-structure PSCs with ITO as the bottom cathode provides a promising approach to address these challenges [5,15]. Key to the cell performance of inverted

* Corresponding authors. Tel.: +86 512 65880942; fax: +86 512 65882846 (J.-X. Tang).
E-mail addresses: yqli@suda.edu.cn (Y.-Q. Li), jxtang@suda.edu.cn (J.-X. Tang).

1566-1199/$ - see front matter © 2012 Elsevier B.V. All rights reserved.
doi:10.1016/j.orgel.2012.01.009

PSCs is the selection of electron collection layers. In recent years, the inverted PSCs showed better long-term air stability in an ambient environment through the use of inorganic materials functioning as an electron collection layer interposed between the ITO cathode and the photoactive layer, such as zinc oxide (ZnO) [16–20], titanium oxide (TiO_x) [21–24], aluminum oxide (Al_2O_3) [25], lithium fluoride (LiF) [26], or cesium carbonate (Cs_2CO_3) [27–29]. In addition, it has been demonstrated that the vertical phase separation spontaneously occurring with the aggregation of fullerene derivatives on the bottom of polymer BHJ results in a favorable morphology in inverted PSC architectures [30]. The employment of inorganic materials, i.e., ZnO and TiO_x as an electron collection layer on the top of ITO cathode is due to their large band gaps and the good electron extraction property. However, a relatively high-temperature annealing process is usually required for the removal of residual organic compounds and crystallization for solution-processed inorganic compound films to achieve well-controlled morphological and structural properties. Such high-temperature processing would inevitably inhibit their application with the flexible substrates [31]. On the other hand, only few attempts have been made for directly using small molecules or conjugated polymers as an electron collection layer for inverted PSCs, because their relatively low conductivities result in high series resistance and poor Ohmic contact with the electrodes [11].

In this work, we report an efficient inverted PSC employing an n-type doped wide-gap organic electron-transporting layer (ETL) for electron extraction, which is formed by a thermal deposition of cesium carbonate-doped 4,7-diphenyl-1,10-phenanthroline (Cs_2CO_3:BPhen) layer. The chemical structure of BPhen molecule is shown in the inset of Fig. 1b. The selection of Cs_2CO_3:BPhen layer as the ETL in the inverted PSC arises from its superior exciton/hole blocking capability, highly optical transparency across the visible spectrum, and electron transporting property due to the large band gap and relatively high electron mobility, as demonstrated in the literatures [32,33]. A correlation between cell response parameters and the film properties of Cs_2CO_3:BPhen layer is investigated, and the enhanced PCE of inverted device is achieved by controlling the doping concentration and film thickness of Cs_2CO_3:BPhen layer. Different from sol–gel chemistry used for the metal oxide films, the approach depositing an n-type doped wide-gap organic ETL for electron extraction offers a convenient and easy method to control film morphology, chemical composition, conductivity at low processing temperature, as well as compatibility with fabrication on flexible substrates.

2. Experimental methods

Inverted PSC as depicted in the inset of Fig. 1b were fabricated on patterned ITO-coated glass substrates with a sheet resistance of 20 Ω/sq. Prior to device fabrication, the ITO glass substrates were ultrasonic cleaned with Decon 90, rinsed in de-ionized water, and dried in an oven. Then, the substrates were transferred to a vacuum deposition chamber with a base pressure of 2×10^{-6} Torr for

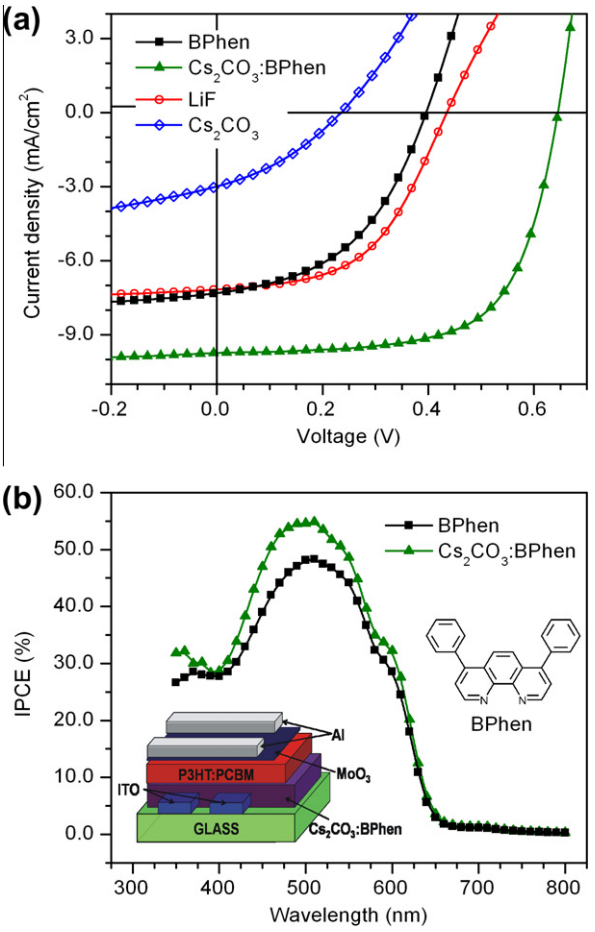

Fig. 1. (a) J–V characteristics of inverted P3HT:PCBM solar cells incorporating Cs_2CO_3, LiF, BPhen, and Cs_2CO_3:BPhen as an ETL under 100 mW cm^{-2} AM 1.5 G irradiation. (b) IPCE spectra of inverted solar cells with BPhen and Cs_2CO_3:BPhen as an ETL. The inset in (b) shows the chemical structure of BPhen and the inverted device configuration.

thermal evaporation of Cs_2CO_3-doped BPhen layers with various host-dopant compositions and film thicknesses, which were produced by co-evaporation from individual Cs_2CO_3 and BPhen sources. Deposition rates and thicknesses of different layers were monitored with a quartz oscillating crystal, which was calibrated initially. After thermal deposition of Cs_2CO_3:BPhen, the resulting samples were transferred into a nitrogen (N_2)-filled glove box for the preparation of the photoactive layer of poly(3-hexylthiophene):[6,6]-phenyl C61 butyric acid methyl ester (P3HT:PCBM) blend, which was spin-coated from a 1:08 weight-ratio chlorobenzene-based solution (20 mg mL^{-1}) onto Cs_2CO_3:BPhen coated ITO substrates, and heated at 150 °C for 30 min inside the glove box. The thickness of the resultant P3HT:PCBM blend film was determined to be approximately 120 nm by the alpha-SE™ Spectroscopic Ellipsometer. Finally, the samples were transferred back to the vacuum deposition chamber to complete the inverted PSC devices, in which a 2 nm-thick molybdenum oxide (MoO_3) layer as a hole collection layer and a 100 nm-thick Al anode were thermally evaporated through shadow

masks. The active device area was 0.1 cm^2 determined by the overlap of ITO cathode and Al anode.

Photovoltaic measurements were conducted at room temperature in air without any device encapsulation under the illumination of an 150 W Newport 91160 solar simulator using an air mass (AM) 1.5 G filter. The simulated light intensity was adjusted to be 100 mW cm^{-2}, which was calibrated with a calibrated silicon solar cell. The current density–voltage (J–V) characteristics of the inverted PSC devices were examined with a programmable Keithley 2612 source meter. The incident photon to current conversion efficiency (IPCE) spectra were measured with a photomodulation spectroscopic setup (Newport monochromator). Surface morphology and roughness were characterized with atomic force microscopy (AFM) (Veeco MultiMode V) in tapping mode. The UV–vis absorption and transmission measurements of the samples were recorded at room temperature with a Perkin Elmer Lambda 750 UV/Vis/NIR spectrophotometer. X-ray and ultraviolet photoemission spectroscopies (XPS and UPS) were performed in a Kratos AXIS Ultra-DLD ultrahigh vacuum system, which is composed of a fast entry air lock, a multiport carousel chamber, an evaporation chamber, and an analysis chamber. The base pressures in the four chambers were better than 1×10^{-8}, 5×10^{-10}, 5×10^{-10}, and 3×10^{-10} Torr, respectively. XPS measurement with monochromatic Al K_α source ($h\nu$ = 1486.6 eV) was used to determine the interfacial chemical reactions. UPS analysis was performed to characterize the valence states and vacuum level (VL) with an unfiltered He I ($h\nu$ = 21.22 eV) gas discharge lamp and a total instrumental energy resolution of 100 meV. During the UPS measurement, samples were negatively biased for the observation of secondary electron cutoff. All spectra were measured at room temperature. Fermi level (E_F) was referred as the zero binding energy (BE) in XPS and UPS spectra.

3. Results and discussion

Fig. 1a plots the J–V characteristics of inverted PSCs incorporating a 30 nm-thick Cs_2CO_3:BPhen layer (doping ratio = 10 wt.%) as the ETL. For comparison, the J–V properties of inverted devices incorporating respectively a thermally deposited 1 nm-thick Cs_2CO_3, 1 nm-thick LiF, or 30 nm-thick BPhen layer as the ETL are also shown in Fig. 1a. Note that devices with pristine BPhen, LiF or Cs_2CO_3 as an ETL show poor short-circuit current density (J_{SC}), open-circuit voltage (V_{OC}), and fill factor (FF), implying that they provide the inferior function in terms of electron extraction and transport to the cathode. In contrast, inverted PSC incorporating a Cs_2CO_3:BPhen layer exhibits a significantly enhanced photovoltaic response with J_{SC} of 9.74 mA cm^{-2}, V_{OC} of 0.64 V, and FF of 66%, and thus an enhanced PCE of 4.12% under 100 mW cm^{-2} AM 1.5 G simulated solar illumination.

IPCE spectra or external quantum efficiency (EQE) of inverted PSCs with pristine BPhen and Cs_2CO_3:BPhen as an ETL are compared in Fig. 1b. It shows that the IPCE for inverted device with a Cs_2CO_3:BPhen ETL is higher than that with a pristine BPhen layer, which is consistent with the J–V behaviors as plotted in Fig. 1a. However, the negligible difference in shape of the IPCE spectra is indicative of similar morphology and crystallinity degree of P3HT:PCBM BHJ in these two PSCs. Therefore, the performance enhancement is associated with Cs_2CO_3 doping in BPhen ETL instead of the effect of P3HT:PCBM active layer.

The morphology of the ETL is an important factor that governs device performance since the formation of P3HT:PCBM active layer is rather sensitive to the underlying interfacial layer and a smooth and pinhole-free ETL film prevents the leakage current at the interface. The topography and surface roughness of the 30 nm-thick Cs_2CO_3:BPhen and the 120 nm-thick P3HT:PCBM blend on the top of Cs_2CO_3:BPhen were investigated by AFM. As shown in Fig. 2a and c, there is negligible difference in the morphology of pristine BPhen and Cs_2CO_3:BPhen layers by thermal deposition in vacuum, and the surfaces of both layers are smooth and contiguous with the root mean square (RMS) roughness values of 0.35 and 0.38 nm, respectively. Meanwhile, Fig. 2b and d shows that the morphologies of the P3HT:PCBM layers spin-coated on pristine BPhen and Cs_2CO_3:BPhen layers are almost identical with an average RMS roughness of 1.7 nm, implying that the Cs_2CO_3 doping in BPhen layer has no significant influence on film morphology of the P3HT:PCBM blend. This is in good agreement the observation of the IPCE spectra in Fig. 1b. Moreover, there is no obvious variation of the UV–vis absorption spectra for P3HT:PCBM blends spin-coated pristine BPhen and Cs_2CO_3:BPhen layers (not shown here). It further demonstrates that the performance enhancement for inverted device with a Cs_2CO_3:BPhen ETL is not related to incident light loss delivered to the active region under illumination.

To identify the origin of the enhanced performance induced by the Cs_2CO_3 doping in the BPhen layer, electronic structures at the BPhen/P3HT:PCBM and Cs_2CO_3:BPhen/P3HT:PCBM interfaces were examined by XPS and UPS measurements. It is verified by XPS measurement (see Fig. 3) that Cs_2CO_3 decomposes into cesium oxide during thermal evaporation, whereas no strong chemical reaction occurs between Cs_2CO_3 and BPhen in the doping system [34].

Fig. 4 displays the zoom-in plots of the secondary electron cutoff (left panel) and the highest occupied molecular orbital (HOMO) regions (right panel) of HeI UPS spectra for pristine BPhen, Cs_2CO_3:BPhen, and P3HT:PCBM blend spin-coated on the former two substrates, respectively. Vertical bars in the right panel of Fig. 4 mark the HOMO edges of the corresponding films. The pristine BPhen and Cs_2CO_3:BPhen (10 wt.%) layers with a thickness of 10 nm were *in situ* thermally deposited onto ITO substrates in the evaporation chamber, and transferred to the analysis chamber for UPS measurements without breaking the vacuum. The P3HT:PCBM blends were *ex situ* spin-coated onto pristine BPhen and Cs_2CO_3:BPhen layers. As shown in Fig. 4, the Cs_2CO_3 doping into the BPhen layer causes a rigid shift of all the UPS spectral features towards higher binding energy, indicating the E_F movement within the energy gap towards the lowest unoccupied molecular orbital (LUMO) of BPhen. The HOMO edge of pristine BPhen or Cs_2CO_3:BPhen layer is estimated to be at 3.4 or 4.0 eV below E_F, respectively. Taking into account the energy gap of 4.2 eV for BPhen obtained by combining UPS and inverse photoelec-

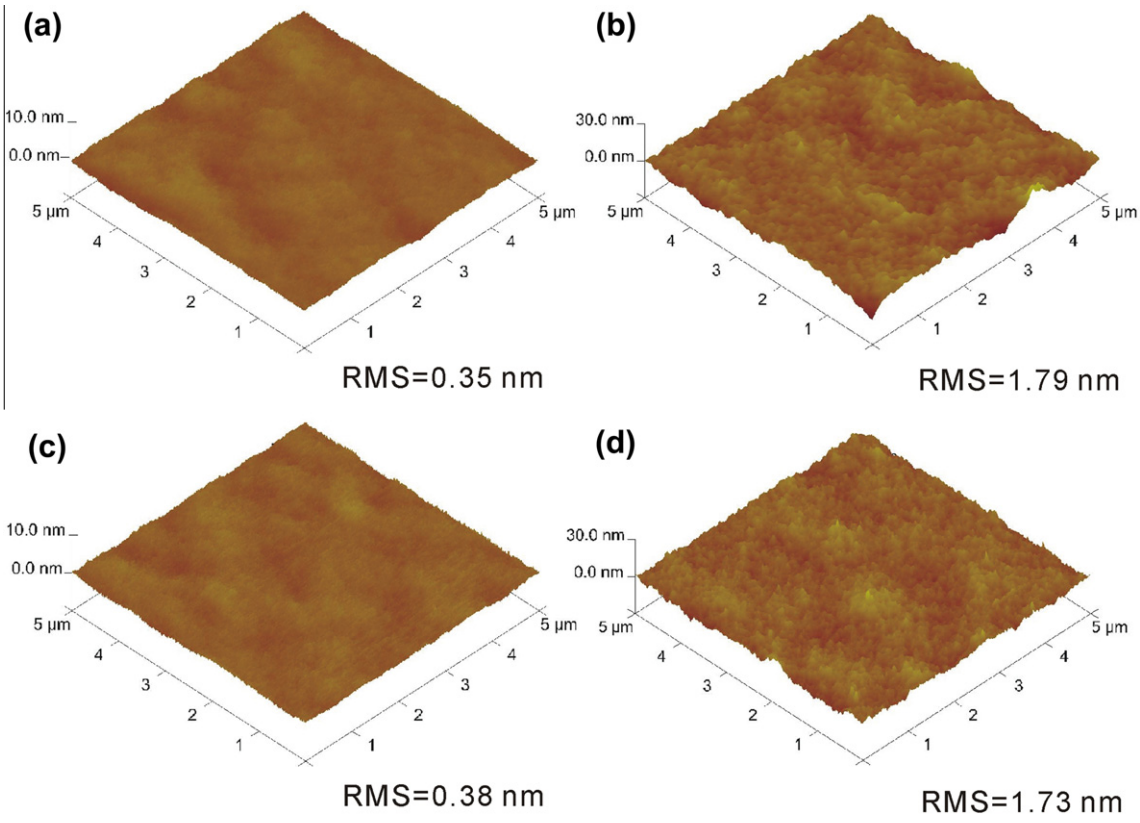

Fig. 2. AFM images of (a) BPhen, (b) P3HT:PCBM on BPhen, (c) Cs_2CO_3:BPhen, and (d) P3HT:PCBM on Cs_2CO_3:BPhen.

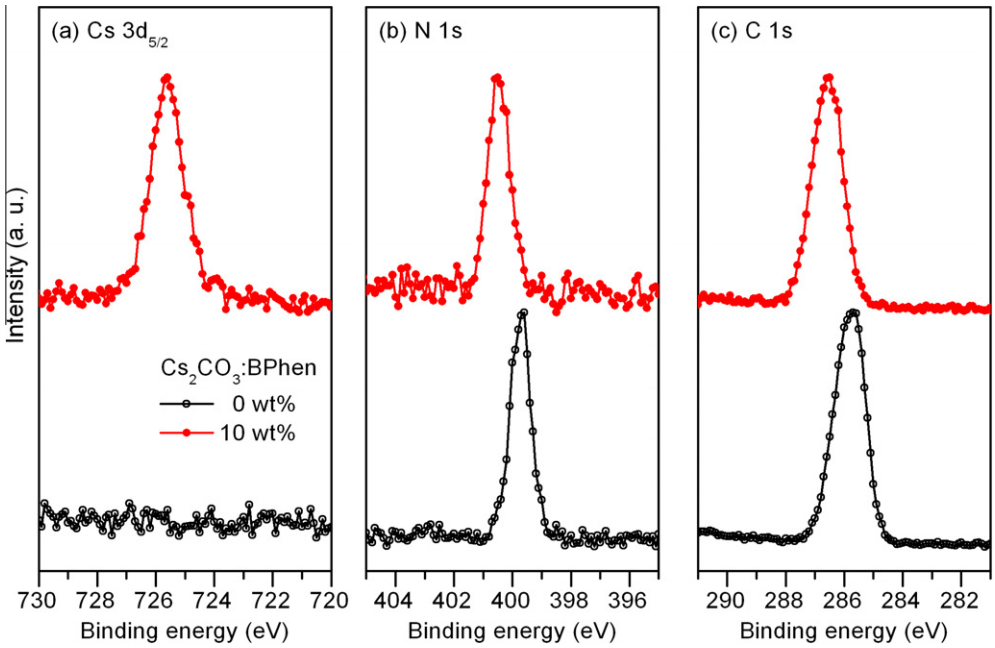

Fig. 3. XPS spectra of (a) Cs $3d_{5/2}$, (b) N 1s, and (c) C 1s core levels for pristine BPhen and Cs_2CO_3:BPhen (10 wt.%) film.

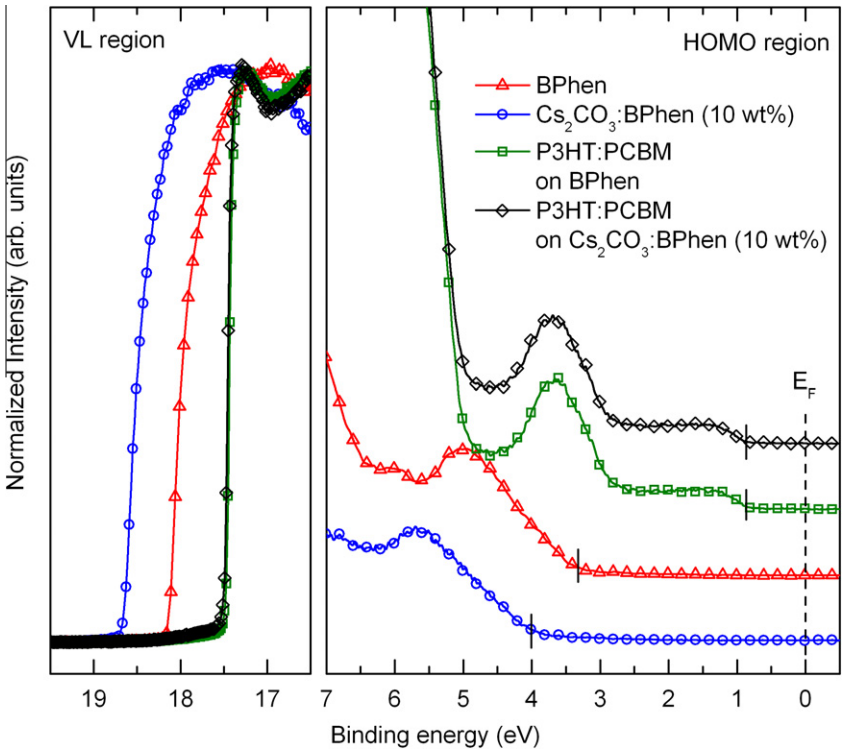

Fig. 4. HeI UPS spectra of BPhen and Cs_2CO_3:BPhen (10 wt.%) layers *in situ* deposited on ITO substrates, and P3HT:PCBM active layer spin-coated on a Cs_2CO_3:BPhen layer: (left panel) normalized secondary electron cutoff region and (right panel) enlarged HOMO region.

tron spectroscopy [35], the LUMO of pristine BPhen and Cs_2CO_3:BPhen layers should be 0.8 and 0.2 eV above E_F, implying E_F pinning to the LUMO edge induced by Cs_2CO_3 doping. In addition, the VL can be determined by the intercept between the background level and the extrapolation of the secondary electron cutoff, while the shift of the secondary electron cutoff corresponds to the decrease of the work function of the Cs_2CO_3:BPhen layer relative to that of pristine BPhen, which is in good agreement with the previous reports [34]. According to the UPS spectra in Fig. 4, the work function of pristine BPhen on ITO substrate is determined to be 3.1 eV, while the corresponding work function of the Cs_2CO_3:BPhen layer is reduced to about 2.6 eV.

On the other hand, Fig. 4 shows that the UPS spectra of P3HT:PCBM blend spin-coated on pristine BPhen or Cs_2CO_3:BPhen layers are almost identical with negligible energy shift, although the spectral features are dominated by the P3HT component due to vertical phase separation with the accumulation of P3HT at the blend surface [36]. The work function of the P3HT:PCBM blend extracted from the UPS spectra is about 3.7 eV, while the HOMO edge of P3HT is at 0.9 eV below E_F.

Using the results from UPS measurements, the direct energy level alignment at the interface can be accurately determined. Fig. 5 illustrates the schematic energy level diagrams of the component materials used in the inverted configuration on ITO substrate with E_F alignment. The VL and HOMO energies relative to E_F are extracted from UPS measurements, and the LUMO energies are derived from HOMO plus energy gaps. Due to vertical phase separation in blended P3HT:PCBM layers [36], the energy levels of PCBM cannot be directly determined from the UPS spectra, but are estimated via VL alignment with that of P3HT. It is noted that the energy offsets at BPhen/P3HT:PCBM and Cs_2CO_3:BPhen/P3HT:PCBM interfaces are remarkably different from the predicted values under the rule of VL alignment due to interface dipole formation. As shown in Fig. 5b, the Cs_2CO_3 doping in BPhen can give rise to the downward shift of BPhen's HOMO and LUMO levels, causing the well-aligned LUMO levels between Cs_2CO_3:BPhen and the electron acceptor PCBM in the polymer BHJ active layer. Therefore, electron extraction at the Cs_2CO_3:BPhen/PCBM interface is expected to be highly efficient due to reduction of the electron barrier height. This is consistent with the photovoltaic response shown in Fig. 1a, in which an Ohmic contact between the active layer and the ITO cathode is formed with the insertion of Cs_2CO_3:BPhen layer leading to an increase in V_{OC}. In addition, the Cs_2CO_3 doping in the BPhen layer can increase the carrier density and conductivity in Cs_2CO_3-doped BPhen layer, which is helpful for electron transport to the ITO cathode. On the other hand, the Cs_2CO_3:BPhen can function as a hole blocking layer to prevent the loss of holes to the cathode as well, owing to the large HOMO offset between Cs_2CO_3:BPhen and P3HT. These results clearly demonstrate that Cs_2CO_3:

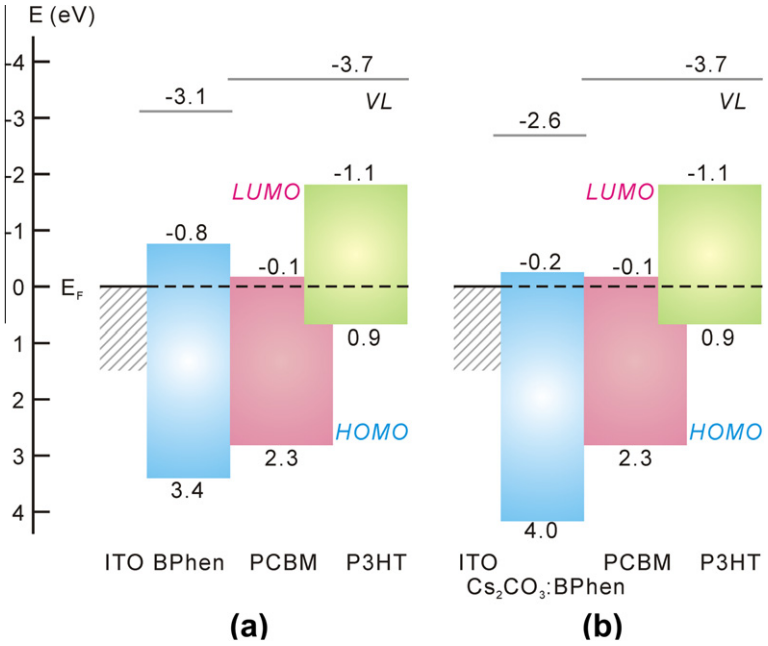

Fig. 5. Schematic energy level diagrams of the component materials used in the inverted configuration on ITO substrate with the Fermi level (E_F) alignment. (a) ITO/BPhen/P3HT:PCBM and (b) ITO/Cs_2CO_3:BPhen/P3HT:PCBM structures.

BPhen can effectively function as an ETL in the inverted PSCs.

To further examine the impacts of Cs_2CO_3:Bphen ETL on device performance, two series of inverted PSCs incorporating Cs_2CO_3:BPhen as an ETL were fabricated as a function of doping concentration and film thickness of the Cs_2CO_3:BPhen layer, respectively. To minimize effects due to different processing conditions, all the devices in each series were fabricated during the same batch processing. Fig. 6a plots the J–V characteristics of inverted PSCs incorporating a 30 nm-thick Cs_2CO_3:BPhen ETL with different Cs_2CO_3 doping concentrations under AM 1.5 G irradiation at an intensity of 100 mW cm^{-2}. The extracted device parameters are summarized in Table 1. The results clearly show the evolution of J–V curves of inverted PSCs as a function of the doping concentration of Cs_2CO_3. As shown in Table 1, the photovoltaic parameters of FF, V_{OC}, and J_{SC} increase significantly with an overall decrease in series resistance (R_S) when the Cs_2CO_3 doping concentration is increased from 0 to 10 wt.%. The device incorporating a Cs_2CO_3:BPhen ETL with a doping concentration of 10 wt.% yields the best performance with a maximum PCE of 4.12%, which is over three times that of the device with a pristine BPhen ETL.

Fig. 7 shows the UPS spectra of 10 nm-thick Cs_2CO_3:BPhen films with various Cs_2CO_3 doping concentrations, which are in good agreement with previous report [34]. As depicted in Fig. 7, the increase in Cs_2CO_3 doping concentration induces a gradual shift of E_F movement towards LUMO, implying the reduction of the electron injection barrier and the increase of the carrier density for Cs_2CO_3:BPhen films. Fig. 8 displays the J–V characteristics of the electron-only devices with a structure of ITO/Cs_2CO_3:BPhen/Al, in which positive voltage was applied to the bottom ITO contact. The electrical conductivities are shown in Table 1. With respect to the increase of the Cs_2CO_3 doping concentration, the J–V characteristics exhibit a linear relationship at positive and negative voltage, indicating the Ohmic contact of the Cs_2CO_3:BPhen layer with Al or ITO electrodes. In addition, it is noted that the current density for a given voltage increases with Cs_2CO_3 doping concentration, demonstrating the improved conductivity of the Cs_2CO_3-doped electron transport layer. For example, the conductivity of the Cs_2CO_3:BPhen layers as determined from Fig. 8 was enhanced from 0.92×10^{-6} to 1.62×10^{-6} S cm^{-1} when the doping concentration was increased from 10 to 30 wt.%.

According to the UPS spectra and charge carrier transport measurements shown in Figs. 7 and 8, the improvement in the inverted device is attributed to the improved electron extraction efficiency of Cs_2CO_3:BPhen induced by the reduction of the electron barrier height at the interface between Cs_2CO_3:BPhen and PCBM as well as the enhanced electrical conductivity in Cs_2CO_3:BPhen layer as a result of increased Cs_2CO_3 doping concentration. However, it is also noted that further increase of the Cs_2CO_3 doping concentration to more than 10 wt.% will lead to the decrease of the device performance with lower J_{SC}, V_{OC}, and FF. For instance, the inverted device incorporating a Cs_2CO_3:BPhen layer with a doping concentration of 30% shows a PCE of 2.59%. The reduction in device performance is because higher doping concentration induces saturated electron barrier height but more electron trapping sites, which is disadvantageous for photocurrent transport [34].

Fig. 6b plots the J–V characteristics of inverted PSCs incorporating a Cs_2CO_3:BPhen (10 wt.%) ETL with various film thicknesses. A summary of the photovoltaic parame-

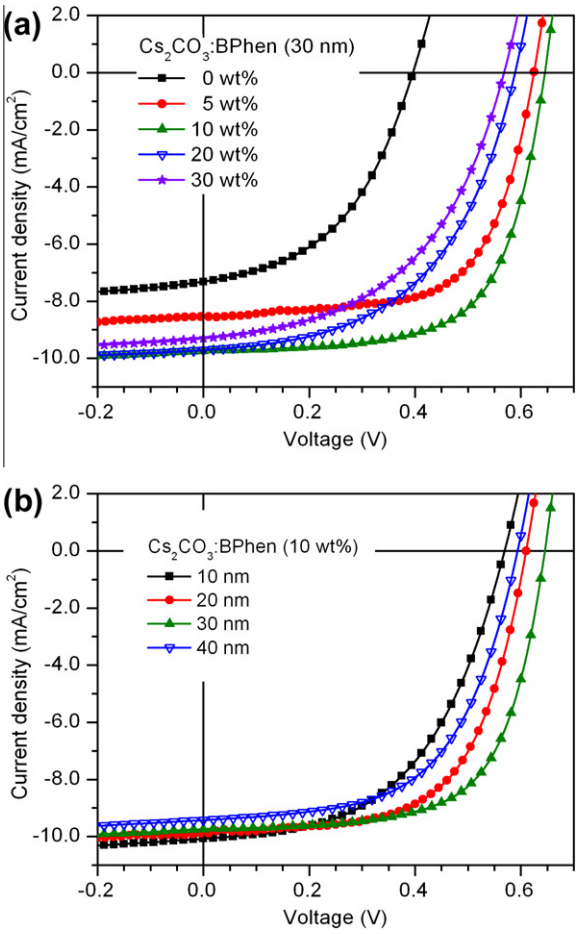

Fig. 6. J–V characteristics of inverted P3HT:PCBM PSCs under 100 mW cm^{-2} AM 1.5 G irradiation as a function of (a) Cs_2CO_3 doping concentration and (b) film thickness of the Cs_2CO_3:BPhen ETL.

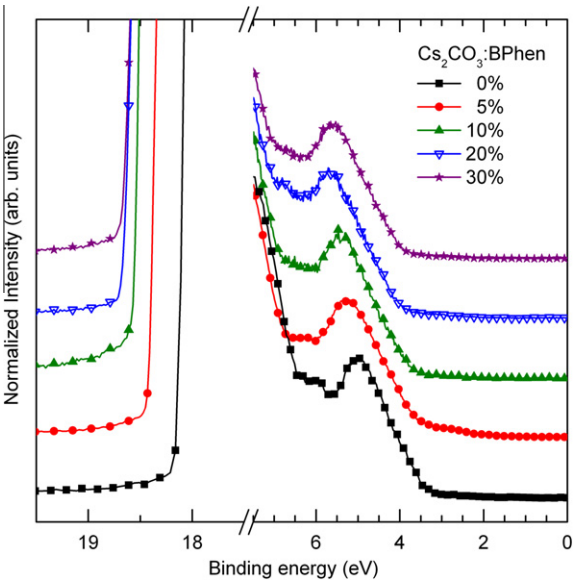

Fig. 7. HeI UPS spectra of 10 nm-thick Cs_2CO_3:BPhen layers *in situ* deposited on ITO substrates for various Cs_2CO_3 doping concentrations.

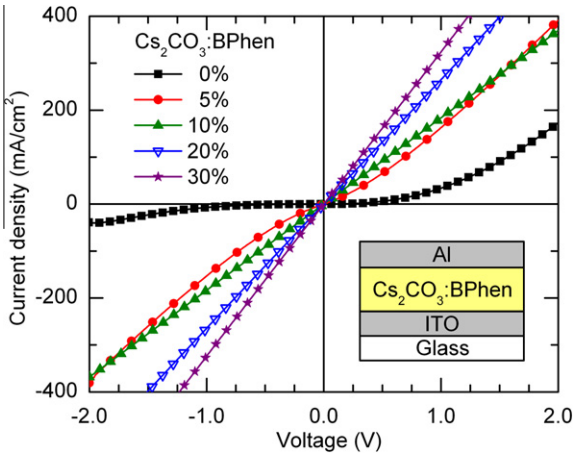

Fig. 8. J–V characteristics of electron-only Cs_2CO_3:BPhen devices as a function of Cs_2CO_3 doping concentration. The device structure is ITO/Cs_2CO_3:BPhen (×wt.%, 50 nm)/Al (100 nm).

ters for the inverted devices with different Cs_2CO_3:BPhen thicknesses is also given in Table 1. It is observed that when the Cs_2CO_3:BPhen thickness is lower than 10 nm, the device exhibits a poor performance, resulting in J_{SC} of 10.07 mA cm^{-2}, V_{OC} of 0.57 V, fill factor (FF) of 52%, and PCE of only 2.96%. However, the inverted devices shows a significant improvement with increasing Cs_2CO_3:BPhen thickness, which is reflected by the larger V_{OC}, larger FF, and higher PCE. The device with a 30 nm-thick Cs_2CO_3:BPhen layer yields the best device performance. The major improvement in device performance with the incorporation of a 30 nm-thick Cs_2CO_3:BPhen layer is due to the higher FF and V_{OC}, although a slightly lower J_{SC} is observed.

Table 1
Device performance parameters of inverted P3HT:PCBM solar cells incorporating a Cs_2CO_3:BPhen ETL with various Cs_2CO_3 doping ratios and film thicknesses, and the electrical conductivities of Cs_2CO_3:BPhen layers.

Thickness [nm]	Ratio [wt.%]	V_{OC} [V]	J_{SC} [mA cm^{-2}]	FF [%]	PCE [%]	R_S [Ω]	Conductivity [S cm^{-1}]
30	0	0.39	7.31	47	1.34	158.42	$0.01–0.10 \times 10^{-6}$
30	5	0.62	8.54	65	3.42	31.22	$0.45–0.90 \times 10^{-6}$
30	10	0.64	9.74	66	4.12	22.32	0.92×10^{-6}
30	20	0.59	9.71	52	2.94	30.13	1.33×10^{-6}
30	30	0.56	9.30	50	2.59	31.56	1.62×10^{-6}
10	10	0.57	10.07	52	2.96	43.51	–
20	10	0.60	9.90	62	3.70	33.48	–
40	10	0.50	9.43	57	3.21	31.25	–

In addition, further increase of Cs_2CO_3:BPhen thickness above 30 nm leads to a reduction in J_{SC}, V_{OC}, and FF. The dependence of the resultant device performance on the Cs_2CO_3:BPhen thickness is well matched with the trend of R_S. As shown in Table 1, the R_S decreases to a minimum at a Cs_2CO_3:BPhen thickness of 30 nm, and then increases with a thicker Cs_2CO_3:BPhen layer. At the same time, the increased R_S can lead to a reduction in FF and V_{OC}, hence a reduction in PCE. Therefore, the results in Fig. 6 confirm that the Cs_2CO_3:Bphen ETL with the balance between Cs_2CO_3 doping concentration and film thickness is critical to forming an ohmic contact between ITO cathode and the acceptor PCBM for the efficient electron extraction.

4. Conclusions

In summary, efficient inverted polymer solar cells is demonstrated by employing an n-type doped wide-gap organic layer as an ETL, which is composed of Cs_2CO_3-doped BPhen layer. The power conversion efficiency up to 4.12% under 100 mW cm^{-2} AM 1.5 G simulated solar illumination has been achieved in inverted BHJ polymer solar cell by optimizing the film thickness and the doping concentration of the Cs_2CO_3:BPhen layer. The performance enhancement in such inverted polymer solar cells is attributed to desirable energy level alignment at the ITO/Cs_2CO_3:BPhen/PCBM interface, increased conductivity in the Cs_2CO_3:BPhen ETL induced by Cs_2CO_3 doping for efficient electron extraction, as well as the hole blocking capability of Cs_2CO_3:BPhen due to its large band gap. The present device structure provides a facile method for realizing efficient inverted polymer solar cells with easy control of film morphology, chemical composition, and conductivity at low processing temperature.

Acknowledgements

The authors acknowledge the financial support by the National Natural Science Foundation of China (Nos. 91027041, 61007020, 61107022, 61036009, 60937001), National Basic Research Program of China (973 program) (Nos. 2011CB808404, 2010CB934502), the Research Fund for the Doctoral Program of Higher Education of China (Nos. 20093201120019, 20103201120019), the Natural Science Foundation of Jiangsu Province (Nos. BK2011280, BY2009007), and a Project Funded by the Priority Academic Program Development of Jiangsu Higher Education Institutions (PAPD).

References

[1] G. Li, V. Shrotriya, J. Huang, Y. Yao, T. Moriarty, K. Emery, Y. Yang, Nat. Mater. 4 (2005) 864.
[2] S. Günes, H. Neugebauer, N.S. Sariciftci, Chem. Rev. 107 (2007) 1324.
[3] J.Y. Kim, K. Lee, N.E. Coates, D. Moses, T.Q. Nguyen, M. Dante, A.J. Heeger, Science 317 (2007) 222.
[4] G. Dennler, M.C. Scharber, C.J. Brabec, Adv. Mater. 21 (2009) 1323.
[5] L.M. Chen, Z. Hong, G. Li, Y. Yang, Adv. Mater. 21 (2009) 1434.
[6] C.J. Brabec, S. Gowrisanker, J.J.M. Halls, D. Laird, S. Jia, S.P. Williams, Adv. Mater. 22 (2010) 3839.
[7] S.H. Park, A. Roy, S. Beaupré, S. Cho, N. Coates, J.S. Moon, D. Moses, M. Leclerc, K. Lee, A.J. Heeger, Nat. Photonics 3 (2009) 297.
[8] Z.Q. Xu, J. Li, J.P. Yang, P.P. Cheng, J. Zhao, S.T. Lee, Y.Q. Li, J.X. Tang, Appl. Phys. Lett. 98 (2011) 253303.
[9] N. Blouin, A. Michaud, D. Gendron, S. Wakim, M. Belletête, G. Durocher, Y. Tao, M. Leclerc, J. Am. Chem. Soc. 130 (2008) 732.
[10] Y. Liang, Y. Wu, D. Feng, S.T. Tsai, H.J. Son, G. Li, L. Yu, J. Am. Chem. Soc. 131 (2009) 56.
[11] N. Cho, H.L. Yip, S.K. Hau, K.S. Chen, T.W. Kim, J.A. Davies, D.F. Zeigler, A.K.Y. Jen, J. Mater. Chem. 21 (2011) 6956.
[12] W.L. Ma, C.Y. Yang, X. Gong, K. Lee, A.J. Heeger, Adv. Funct. Mater. 15 (2005) 1617.
[13] See Solarmer press release (2011). www.solarmer.com.
[14] C.Y. Li, T.C. Wen, T.H. Lee, T.F. Guo, J.C.A. Huang, Y.C. Lin, Y.J. Hsu, J. Mater. Chem. 19 (2009) 1643.
[15] S.K. Hau, H.L. Yip, A.K.Y. Jen, Polymer Rev. 50 (2010) 474.
[16] M.S. White, D.C. Olson, S.E. Shaheen, N. Kopidakis, D.S. Ginley, Appl. Phys. Lett. 89 (2006) 143517.
[17] J. Gilot, I. Barbu, M.M. Wienk, R.A.J. Janssen, Appl. Phys. Lett. 91 (2007) 113520.
[18] A.K.K. Kyaw, X.W. Sun, C.Y. Jiang, G.Q. Lo, D.W. Zhao, D.L. Kwong, Appl. Phys. Lett. 93 (2008) 221107.
[19] H. Cheun, C. Fuentes-Hernandez, Y.H. Zhou, W.J. Potscavage, S.J. Kim, J. Shim, A. Dindar, B. Kippelen, J. Phys. Chem. C 114 (2010) 20713.
[20] F.C. Krebs, T. Tromholt, M. Jorgensen, Nanoscale 2 (2010) 873.
[21] C. Waldauf, M. Morana, P. Denk, P. Schilinsky, K. Coakley, S.A. Choulis, C.J. Brabec, Appl. Phys. Lett. 89 (2006) 233517.
[22] G.K. Mor, K. Shankar, M. Paulose, O.K. Varghese, C.A. Grimes, Appl. Phys. Lett. 91 (2007) 152111.
[23] M.H. Park, J.H. Li, A. Kumar, G. Li, Y. Yang, Adv. Mater. 19 (2009) 1241.
[24] T. Kuwabara, C. Iwata, T. Yamaguchi, K. Takahashi, ACS Appl. Mater. Interfaces 2 (2010) 2254.
[25] Y.H. Zhou, H. Cheun, W.J. Potscavage, B. Kippelen, J. Mater. Chem. 20 (2010) 6189.
[26] C.J. Brabec, S.E. Shaheen, C. Winder, N.S. Sariciftci, P. Denk, Appl. Phys. Lett. 80 (2002) 1288.
[27] G. Li, C.W. Chu, V. Shrotriya, J. Huang, Y. Yang, Appl. Phys. Lett. 88 (2006) 253503.
[28] H.H. Liao, L.M. Chen, Z. Xu, G. Li, Y. Yang, Appl. Phys. Lett. 92 (2008) 173303.
[29] C.S. Kim, S. Lee, L.L. Tinker, S. Bernhard, Y.L. Loo, Chem. Mater. 21 (2009) 4583.
[30] Z. Xu, L.M. Chen, G. Yang, C.H. Huang, J. Hou, Y. Wu, G. Li, C.S. Hsu, Y. Yang, Adv. Funct. Mater. 19 (2009) 1227.
[31] F.C. Krebs, Sol. Energy Mater. Sol. Cells 93 (2009) 394.
[32] Q.Y. Bao, J.P. Yang, Y.Q. Li, J.X. Tang, Appl. Phys. Lett. 97 (2010) 063303.
[33] M.Y. Chan, C.S. Lee, S.T. Lee, J. Appl. Phys. 100 (2006) 094506.
[34] Y. Cai, H.X. Wei, J. Li, Q.Y. Bao, X. Zhao, S.T. Lee, Y.Q. Li, J.X. Tang, Appl. Phys. Lett. 98 (2011) 113304.
[35] J. Meyer, M. Kröger, S. Hamwi, F. Gnam, T. Riedl, W. Kowalsky, A. Kahn, Appl. Phys. Lett. 96 (2010) 193302.
[36] Z. Xu, L.M. Chen, M.H. Chen, G. Li, Y. Yang, Appl. Phys. Lett. 95 (2009) 013301.